

---

# ROBMOT: ROBUST 3D MULTI-OBJECT TRACKING BY OBSERVATIONAL NOISE AND STATE ESTIMATION DRIFT MITIGATION ON LIDAR POINTCLOUD

---

**Mohamed Nagy**

Electrical and Computer Engineering  
Khalifa University  
mohamed.nagy@ieee.org

**Naoufel Werghi**

Electrical and Computer Engineering  
Khalifa University  
naoufel.werghi@ku.ac.ae

**Bilal Hassan**

Electrical and Computer Engineering  
Khalifa University  
bilal.hassan@ku.ac.ae

**Jorge Dias**

Electrical and Computer Engineering  
Khalifa University  
jorge.dias@ku.ac.ae

**Majid Khonji**

Electrical and Computer Engineering  
Khalifa University  
majid.khonji@ku.ac.ae

May 21, 2024

## ABSTRACT

This work addresses the inherited limitations in the current state-of-the-art 3D multi-object tracking (MOT) methods that follow the tracking-by-detection paradigm, notably trajectory estimation drift for long-occluded objects in LiDAR point cloud streams acquired by autonomous cars. In addition, the absence of adequate track legitimacy verification results in ghost track accumulation. To tackle these issues, we introduce a two-fold innovation. Firstly, we propose refinement in Kalman filter that enhances trajectory drift noise mitigation, resulting in more robust state estimation for occluded objects. Secondly, we propose a novel online track validity mechanism to distinguish between legitimate and ghost tracks combined with a multi-stage observational gating process for incoming observations. This mechanism substantially reduces ghost tracks by up to 80% and improves HOTA by 7%. Accordingly, we propose an online 3D MOT framework, RobMOT, that demonstrates superior performance over the top-performing state-of-the-art methods, including deep learning approaches, across various detectors with up to 3.28% margin in MOTA and 2.36% in HOTA. RobMOT excels under challenging conditions, such as prolonged occlusions and the tracking of distant objects, with up to 59% enhancement in processing latency.

## 1 Introduction

3D Multi-object tracking (MOT) is one of the pillars of autonomous driving. It is responsible for determining the state of objects in the environment, including their spatial location and motion parameters like velocity and acceleration. Trajectory drift has been observed in the state estimation of occluded objects in the top-performing state-of-the-art CasTrack [1], as shown in Figure 1, failing to recover objects under challenging tracking conditions like prolonged occlusion and distant objects emphasized in Figure 6. Our investigation shows this drift comes from fluctuation noise in spatial localization of the objects attached to 3D bounding box detections from deep learning models that tracking-by-detection methods rely on for object localization on LiDAR point cloud. This noise influences the precision

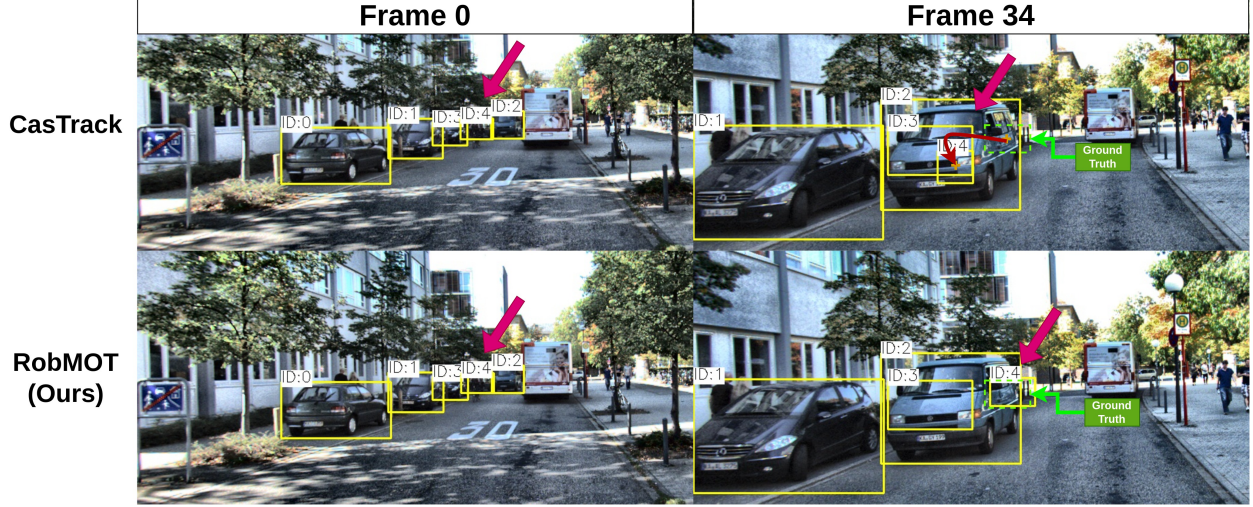


Figure 1: A trajectory drift scenario for a car occluded by a van. The 3D tracking results on the LiDAR point cloud are projected into 2D frames. The first row shows drift in the state estimation of car ID:4 by CasTrack [1] at frame 34 during occlusion caused by fluctuation noise associated with detections before the occlusion. The second row displays the noise mitigation in our proposed solution, resulting in accurate localization of the car during the occlusion. The full stream is provided in a video in the supplemental materials, "Demo.mp4".

of state estimation for spatial location and motion parameters of occluded objects that ultimately deviate from the actual motion trajectory.

Another issue is the absence of trajectory validity verification in the MOT literature [1, 2, 3, 4, 5, 6]. They consider estimated trajectories in the system always legitimate, neglecting ghost trajectories caused by false positive detections. As a result, the literature incorporates a threshold on detection scores of the incoming detections to prevent potential false positive detections. It leaks false positive observations exceeding the threshold while blocking legitimate ones below it for distant and partially occluded objects with low detection scores.

In this work, we refine the state estimation of occluded objects in the Kalman filter by modeling the noise responsible for trajectory drift and incorporating it to update the state in the Kalman, Section 3.2. This refinement mitigates the trajectory drift, allowing the recovery of distant and prolonged occluded objects, as shown in Figure 1. Next, we propose a novel online trajectory validity mechanism for temporal distinguishing between ghost and legitimate tracks, Section 3.3. The mechanism incorporates a multi-stage observational gate that identifies potential detections of legitimate tracks that belong to distant and partially occluded objects to enter the system without being blocked by their low detection score, Section 3.1. The mechanism shows about an 80% reduction in ghost tracks and a 7% enhancement in HOTA. Accordingly, we propose a 3D MOT tracking framework, RobMOT, that combines the innovations of this work. Our contribution can be summarized as follows:

1. To the best of our knowledge, this is the first work to uncover the trajectory drift noise associated with detections and its impact on the state estimation of occluded objects in 3D MOT. *Our refinement in Kalman filter shows superior performance over the top-performing benchmark, CastTrack, on challenging MOT conditions, demonstrated in Figure 6.*
2. We propose a novel online trajectory validity mechanism for temporal distinguishing between ghost and legitimate tracks, supported by a multi-stage observational gate for potential observation identification of the legitimate tracks. *The mechanism reduces about 80% of ghost tracks and enhances HOTA by 7%, as demonstrated in the ablation study Section 4.2.2.*
3. We propose an online 3D MOT framework with exceptional tracking performance, surpassing recent benchmarks to show its robustness across different datasets and detectors. *The framework's performance margin is up to 3.28% in HOTA and 2.36% in MOTA, and the enhancement in computational latency is up to 53%, as demonstrated in Figure 5.*

## 2 Related Work

3D MOT methods on LiDAR point cloud could be categorized into learning and non-learning approaches. Part of learning-based methods in the literature involves end-to-end deep learning models that combine object detection and tracking [7, 8, 9, 10]. Meanwhile, other methods adapt tracking-by-detection paradigm [11, 12, 13, 14] when detections of objects are given and the aim is to perform temporal tracking of the objects. The recent research integrates attention mechanism and transformers concepts [15, 16] into MOT to enhance the tracking performance. However, learning-based solutions require evolved hardware to be applicable for real-time applications.

Meanwhile, non-learning MOT solutions [4, 5, 2, 3, 6, 17, 1] have gained much attention due to their low latency and the comparative performance with learning-based solutions. Despite the recent advancement in non-learning methods, object occlusion and ghost tracks remain challenging, particularly in autonomous driving applications where the environment frequently evolves.

**Kalman filter** (KF) is widely used in tracking-by-detection methods [2, 3, 17, 1] for autonomous driving because of its performance in filtering noise from state estimation while dealing with noisy measurements. If the noise is not appropriately modeled to the filter, it could cause a deviation of the state estimation from the expected state since the filter's estimation is sensitive to imprecise measurements. Cao et al. [6] prevents error accumulation in the state prediction caused by periodic occlusion of objects by refining the object's trajectory by addressing the accumulated errors during occlusion. However, successfully recovering the object after occlusion is required to refine the trajectory. Because of the point cloud's sparsity, the incoming detections from 3D detectors suffer from spatial distortion around the object's actual location. This spatial distortion results in an imprecise estimation of the motion parameters, ultimately leading to a deviation in the state estimation once the object faces an occlusion. **Ghost tracks** are false positive detections generating illusion tracks that could eventually lead to wrong navigation of the AV. Since the tracking-by-detection paradigm relies heavily on detection accuracy, ghost tracks in object tracking can significantly harm the tracking performance. Kim et al. [3] introduce a multi-stage data association method to overcome this issue by employing multiple detection sources. Nevertheless, they still depend on predefined thresholds to prevent false positives. The downside of a fine-tuned threshold while filtering ghost tracks is the potential of leaking false positive detections that exceed the threshold while blocking detections that belong to actual tracks. Other approaches [5, 2] incorporate a filtration step to address false positive detections. Wang.X et al. [2]

confirm the legitimacy of a track when three consecutive detections of that track have been observed. In contrast, Wang.L et al. [5] select objects for the highest 30% detections in the confidence score. However, the assumptions provided by these solutions may not apply to all scenarios, particularly distant objects or objects subject to periodic occlusions.

**Memory management** plays a critical role in addressing false positive detections. Maintaining ghost tracks in memory can lead to invalid associations. Meanwhile, early elimination may lose legitimate tracks under prolonged occlusion. In the literature, some work [2, 3, 5, 6] set up a threshold to discard tracks from memory based on how long these tracks have not been observed. Although short memory is suitable for ghost track elimination, it could also remove tracks of objects facing prolonged occlusion. On the other hand, long memory will not remove ghost tracks while increasing the computational time. Nagy et al. [17] attempts to address the trade-off by proposing an MOT solution with low latency and leveraging speed to extend the lifetime of objects, thus capturing more occlusion scenarios. While this approach excels in tracking objects with prolonged occlusion, it does not handle false positives. Wu et al. [1] resolve the issue by associating a confidence score to pre-observed objects in object association. This score decreases over time when the object becomes not observed for a period of time to prevent potential associations with false positive detections. Nonetheless, this approach cannot recover objects under prolonged occlusion as their association score will decrease. This work proposes RobMOT, a framework to mitigate state estimation deviation caused by fluctuation noise. It also provides adaptive identification for ghost tracks with a quick elimination from memory alongside a mechanism that prevents legitimate track detections from being blocked while filtering ghost tracks.

## 3 Methodology

As shown in Figure 2, the framework consists of four parts. **A multi-stage observational gate:** Responsible for identifying potential observations of legitimate tracks. **Trajectory innovation and prediction:** Here, a refined Kalman filter updates the state estimation of the trajectories and is used to predict the following state. **Trajectory validity:** Updates the validation of trajectories with new observations based on their current detection score, absence duration, and prior validation score. **Cache:** Holds trajectories stored in the framework and discards terminated tracks.

### 3.1 Multi-Stage Observational Gate

The multi-stage observational gate is an identification step for potential observations of the legitimate tracks identified by the trajectory validity stage, Section 3.3. The primary purpose of this stage is to permit observations of distant

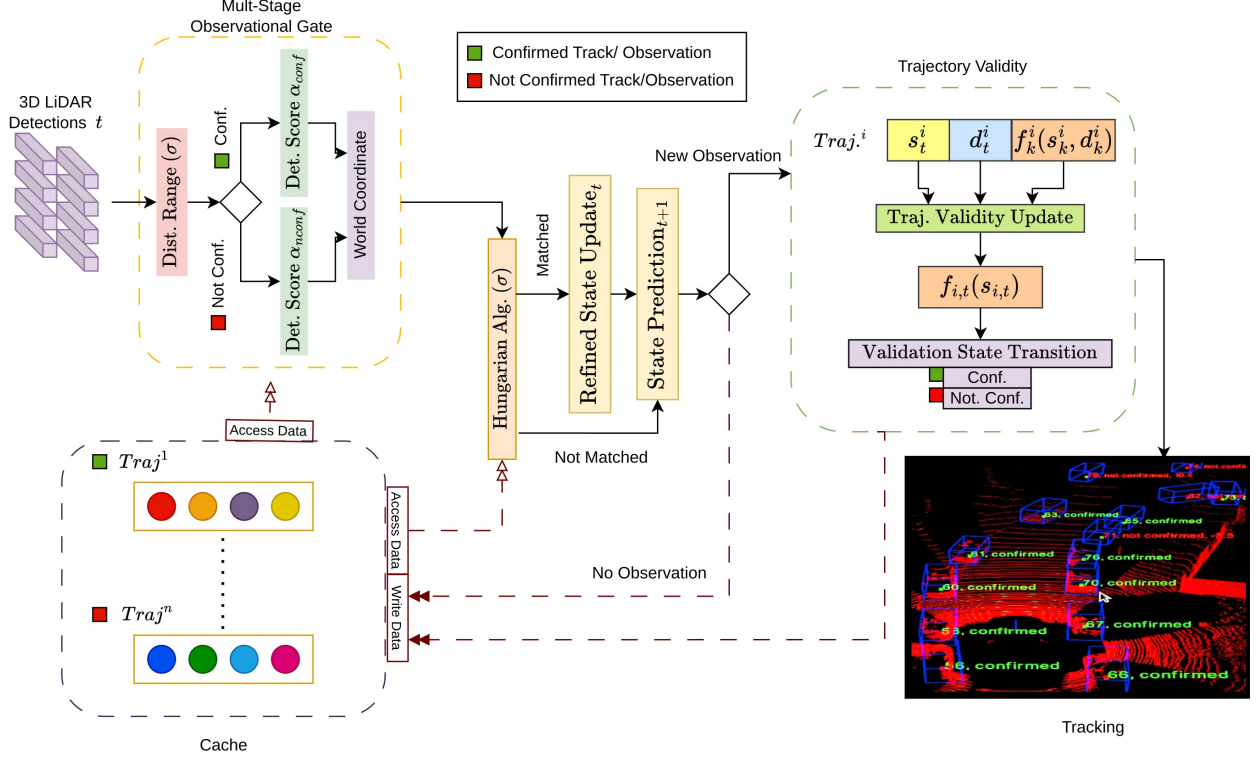


Figure 2: An overview of the RobMOT framework consists of four modules: a **multi-stage observational gate** for identifying legitimate observations, an **association trajectory innovation** for trajectories’ association with observations and next-state prediction, a **trajectory validity** for temporal validation of the trajectories, and a **cache** for storing and termination.

and partially occluded objects with low detection scores to enter the system. Since the trajectory validity stage in Section 3.3 identifies ghost tracks, the first stage of the observational gate is to allow as many new observations to enter the framework as possible with a detection score higher than or equal to  $\alpha_{nconf}$ . The purpose of  $\alpha_{nconf}$  is that numerous detections could harm the latency of the framework and association, so  $\alpha_{nconf}$  limits the detections outpouring. However, some of the detections outpouring prevented by the first stage using  $\alpha_{nconf}$  may contain detections of legitimate tracks. Hence, the second stage aims to permit the potential observation of legitimate tracks, legitimate observations, with detection scores lower than  $\alpha_{nconf}$ . First, it determines the legitimate observations when the Euclidean distance of the centroid point between the observation and one of the verified trajectories, from the trajectory validity stage, is under the same threshold  $\sigma$  distance used in the association step in Section 3.2. The identified legitimate observations pass through additional detection  $\alpha_{conf}$  score filtration when  $\alpha_{conf} \leq \alpha_{nconf}$  to prevent miss identified legitimate observations from entering the framework. Since some non-legitimate observations could have a distance less than  $\sigma$  with a legitimate track,  $\alpha_{nconf}$  aims to prevent these observations from entering the system. Lastly, the filtered observations are projected from the LiDAR coordinate to the world coordinate.

### 3.2 Trajectory Association and State Estimation

Once the Observational Association Gate has filtered the observations, the state estimation of trajectories in the cache is associated with the detections by Hungarian algorithm. Each state estimation of a trajectory is associated with an observation with the least Euclidean distance. Once the least distance exceeds  $\sigma$ , the algorithm terminates. Observations with no matching are considered new tracks. Next, the state update and prediction of trajectories are done by KF. If a trajectory state estimation is matched with an observation, the state estimation will pass by state update and state prediction, as illustrated in Figure 2. Trajectories with no matched state estimation will pass directly to state prediction to predict the next state using the last motion parameters. In this work, the framework uses Kalman filter with constant acceleration, which means the acceleration prediction of the following state will be the same as the last. However, the acceleration will be updated with new observations in the update state.

Since our objective is to mitigate noise associated with the detections shown in Figure 1, which is a distortion/fluctuation



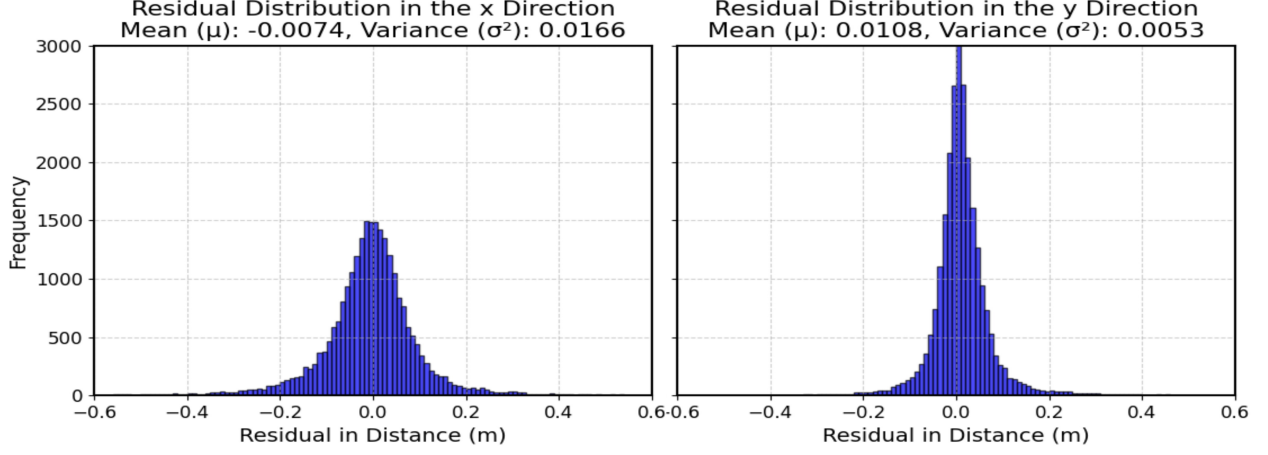


Figure 3: The distribution of the fluctuation noise associated with VirConv [18] detections. The distribution shows Gaussian noise across five different detectors [18, 19, 20, 21, 22]; refer to the supplementary materials for figures of the other four detectors.

around the actual spatial location, we start by modeling the noise distribution by computing the algebraic deviation between the detection bounding box spatial location  $x_i^{det}$  of object  $i$  and the actual location  $x_i^{gt}$  from the ground truth across all observations for that object, denoted by  $k_i$ . Equation 1 computes the algebraic deviation for  $N$  objects. Next, the mean of the algebraic deviation  $\mu_x$  is used to calculate the noise variance across the x coordinate, Equation 1.

$$\begin{aligned}\mu_x &= \frac{1}{\sum_{i=1}^N k_i} \sum_{i=1}^N \sum_{j=1}^{k_i} (x_{ij}^{gt} - x_{ij}^{det}) \\ \sigma_x^2 &= \frac{1}{\sum_{i=1}^N k_i} \sum_{i=1}^N \sum_{j=1}^{k_i} ((x_{ij}^{gt} - x_{ij}^{det}) - \mu_x)^2\end{aligned}\tag{1}$$

By repeating the procedures on the y coordinate, a covariance matrix can be obtained, Equation 2.

$$\mathbf{D} = \begin{bmatrix} \sigma_x^2 & 0 \\ 0 & \sigma_y^2 \end{bmatrix}\tag{2}$$

The noise distribution shows Gaussian distribution across various detectors, as shown in Figure 3, which facilitates integrating the noise into KF.

The deviation noise impacts the observation  $z_t$ , which is used to compute the residual  $\hat{y}_t$  with the state estimation  $\hat{x}_{t|t-1}$  predicted at  $t - 1$ . Since the innovation covariance  $S_t$  is responsible for weighting the innovation residual  $\hat{y}_t$  through Kalman gain  $K_t$ , the noise covariance  $D_t$  will be added to the innovation covariance  $S_t$ . Hence, the updated state estimation  $\hat{x}_{t|t}$  will consider the impact of the deviation noise on the observation. The main reason for not using  $R_t$  instead is because it models the incorrectness of the measurement for the point cloud from LiDAR with respect to the real world, while  $D_t$  models the incorrectness of the detection process with respect to the LiDAR point cloud, which means they are independent. Equation 3 demonstrates the updated state of KF after adapting  $D_t$  noise.

$$\begin{aligned}\text{Innovation Residual: } \tilde{y}_t &= z_t - H_t \hat{x}_{t|t-1} \\ \text{Innovation Covariance: } S_t &= H_t P_{t|t-1} H_t^T + R_t + D_t \\ \text{Kalman Gain: } K_t &= P_{t|t-1} H_t^T S_t^{-1} \\ \text{State Estimation Update: } \hat{x}_{t|t} &= \hat{x}_{t|t-1} + K_t \tilde{y}_t \\ \text{Estimation Covariance Update: } P_{t|t} &= (I - K_t H_t) P_{t|t-1}\end{aligned}\tag{3}$$

$H_t$  is the observation model to map from estimation to measurement space at time  $t$ , while  $P_{t|t-1}$  is the estimation uncertainty at time  $t$  given measurement at  $t - 1$ . In Section 3.4,  $P_{t|t}$  will contribute to trajectory termination in the cache.

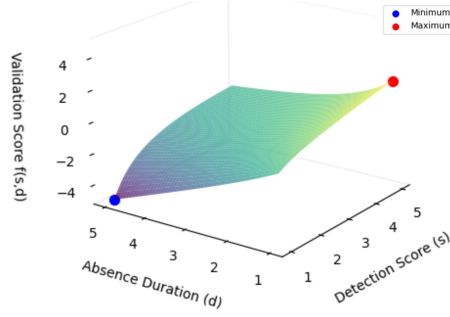


Figure 4: A graphical visualization of the validation scoring formula over detection scores of range  $[0, 5]$  and absence duration  $[0, 5]$  frames. The **red point** is the highest possible outcome of the formula when the detection score is highest while the absence duration is at the lowest value. In contrast, the **blue point** is the lowest outcome when the detection score is at the lowest value, while the absence duration is the highest. The plane diagonal between the two points shows intermediate outcomes.

### 3.3 Trajectory Validity

The framework does temporal validation for a trajectory with every new observation for the trajectory to identify ghost tracks. As per our analysis of the characteristics of the ghost trajectories, these trajectories formed from intermittent observations with low detection scores. However, these characteristics may also be observed in legitimate trajectories with distant observations or undergoing partial to complete occlusion. Hence, online temporal trajectory validity is needed to discriminate legitimate trajectories among trajectories in the system considering ghost trajectory characteristics.

The framework develops certainty  $f_t^i(s_t^i, d_t^i)$  about the legitimacy of a trajectory  $i$  based on detection score  $s_t^i$  attached to its observations at each time  $t$  and the intermittent duration  $d_t^i$  to the last observation at time  $k$ , demonstrated in Equation 4.

$$f_t^i(s_t^i, d_t^i) = s_t^i e^{-d_t^i} - \frac{d_t^i}{s_t^i} + f_k^i(s_k^i, d_k^i) \text{ When } s_t^i > 0 \quad (4)$$

An exponential decay of confidence term is initially added,  $s_t^i e^{-d_t^i}$ , to model a decrease in certainty attached to the current detection score of the observation as time progresses without updates for the trajectory as it becomes less reliable. By degradation in the utilized detector, this term may not be sufficient as the observations of some ghost trajectories can have moderate detection scores that increase its certainty  $f_t^i(s_t^i, d_t^i)$ . Thus, an additional absence duration penalty term is added,  $\frac{d_t^i}{s_t^i}$ , to shrink the certainty of the trajectory as long as the intermittent duration increases. Since some legitimate tracks with high detection scores can suffer from intermittency in the observations during partial occlusion or being distant from the observer, the absence duration penalty is less severe if the recent detection has high detection score confidence.

A visual representation of the distribution of Equation 4 is highlighted in Figure 4; it maximizes when the detection score is at maximum with no absence while minimizing at the lowest detection score and a high absence duration. Lastly, the term  $f_k^i(s_k^i, d_k^i)$  provides temporal validation for the trajectory. The trajectory validation score is computed whenever a new observation is available for that trajectory. If the score exceeds a fine-tuned confirmation threshold, the validation status changes from not confirmed to confirmed. In this case, the trajectory validation process is terminated for that trajectory so that the status cannot change to "not confirmed".

### 3.4 Trajectory Termination and Caching

All trajectory information is saved in a cache module. In the literature, a trajectory is terminated or discarded when the number of frames for the trajectory with no new observation exceeds a certain threshold. Generally, it is not trivial to define an absence threshold as it could risk eliminating objects under occlusion or maintaining a ghost track for long. Instead, in our framework, we discard the trajectory when the estimation uncertainty,  $P_{t|t}$  in Equation 3, becomes high, as it could lead to mismatching during object association. We have observed that ghost tracks tend to have limited observations, leading to high estimation uncertainty. Meanwhile, legitimate tracks maintain low estimation uncertainty, even those under occlusion. Thus, estimation uncertainty is used to terminate tracks from the cache.

## 4 Results and Discussion

The framework has been evaluated on KITTI [23, 24] and Waymo Open Dataset [25] (WOD). KITTI contains a training and evaluation dataset of 21 streams and testing data of 29 streams. Meanwhile, WOD contains about 1150 segments with a smaller stream duration than KITTI. In the following subsections, the framework’s performance will be evaluated quantitatively and qualitatively with the latest top-performing benchmarks on the two datasets in Section 4.1. Next, an ablation study will be conducted to validate the effectiveness of the proposed solutions in the framework, in Section 4.2. All experiments have been conducted on a machine with a processor *AMD Ryzen 9*; no GPU is involved since the framework utilizes CPU only.

### 4.1 Evaluation with Benchmarks

Table 1: Tracking performance on KITTI dataset *testing split* with the latest MOT benchmarks

Method	HOTA	MOTA	MOTP	AssA	AssRe	LocA	IDSW
CasTrack [1]	81.0%	<b>91.9%</b>	86.1%	84.2%	87.6%	87.5%	24
PC-TCNN [26]	80.9%	91.7%	86.1%	84.1%	87.5%	87.5%	37
Rethink MOT [5]	80.1%	91.5%	85.6%	83.6%	87.6%	87.1%	46
MSA-MOT [27]	78.5%	88%	85.5%	82.6%	85.2%	87%	91
DeepFusion-MOT [2]	75.5%	84.6%	85.0%	80.1%	82.6%	86.7%	84
PC3T[28]	77.8%	88.8%	84.3%	81.6%	84.8%	86.1%	225
Mono-3D-KF [29]	75.5%	88.5%	83.7%	77.6%	80.2%	85.5%	162
PolarMOT [30]	75.2%	85.1%	85.63%	76.95%	80%	87.1%	462
TripletTrack[31]	73.58%	84.32%	86.06%	74.66%	77.3%	87.4%	322
RobMOT (Our)	<b>81.8%</b>	91.0%	<b>86.6%</b>	<b>85.6%</b>	<b>89.3%</b>	<b>87.8%</b>	<b>7</b>

The evaluation flow of this work consists of quantitative and qualitative evaluation. Initially, the quantitative evaluation will be conducted on different datasets using the latest MOT benchmarks. Next, the top-performing benchmarks will be selected to be evaluated qualitatively under challenging conditions like occlusion and the performance sensitivity across different detection performances.

#### 4.1.1 Quantitative Evaluation

Table 1 demonstrates the framework’s performance on the KITTI testing dataset. The framework shows superior tracking performance over the benchmarks, including deep learning benchmarks [26], with a about 0.8% margin in HOTA. It shows tracking persistency for objects by having the lowest ID switch (IDSW), 7, compared to the lowest (i.e the best) IDSW achieved by the other benchmarks, 24. Our framework shows improvement in object association (AssA/AssRe) performance with about 1.4% in addition to 0.3% in localization accuracy (LocA). Although the framework excels in MOT precision (MOTP), there is a drop in MOT accuracy of about 0.9% compared to CasTrack [1].

Further evaluation has been conducted on WOD dataset, as demonstrated in Table 2. Table 2 is split into two sections: Level 1 and Level 2 evaluation. Level 1 refers to less challenging tracking conditions compared to Level 2. Our framework shows superior performance in both sections, with a margin of 0.07% in MOTA and a 0.13% reduction in the false positive tracks. Combining the results with Table 1 affirms the superiority of our proposed framework over the recent benchmarks.

Since CasTrack [1] shows superior performance among the benchmarks, we selected the tracker for an intensive study of its tracking performance. First, a sensitive analysis has been conducted with variance in the detection performance. Figure 5 compares tracking performance with CasTrack [1] in HOTA and MOTA metrics across five

Table 2: Tracking performance on Waymo Open dataset *testing split* with the latest MOT benchmarks

	Level 1		Level 2	
Method	MOTA↑	FP↓	MOTA↑	FP↓
CasTrack [1]	66.95%	7.74%	63.66%	7.36%
ImmotralTrack [32]	63.77%	8.94%	60.55%	8.48%
SimpleTrack [33]	63.53%	8.66%	60.30%	8.75%
CenterPoint [34]	62.58%	9.03%	59.38%	9.41%
AlphaTrack [35]	58.86%	10.10%	55.67%	9.55%
RobMOT (Ours)	<b>67.02%</b>	<b>7.60%</b>	<b>63.67%</b>	<b>7.22%</b>

detectors: VirConv [18], CasA [19], PointRCNN [21], PV-RCNN [22], and Second [20]. The study shows a significant

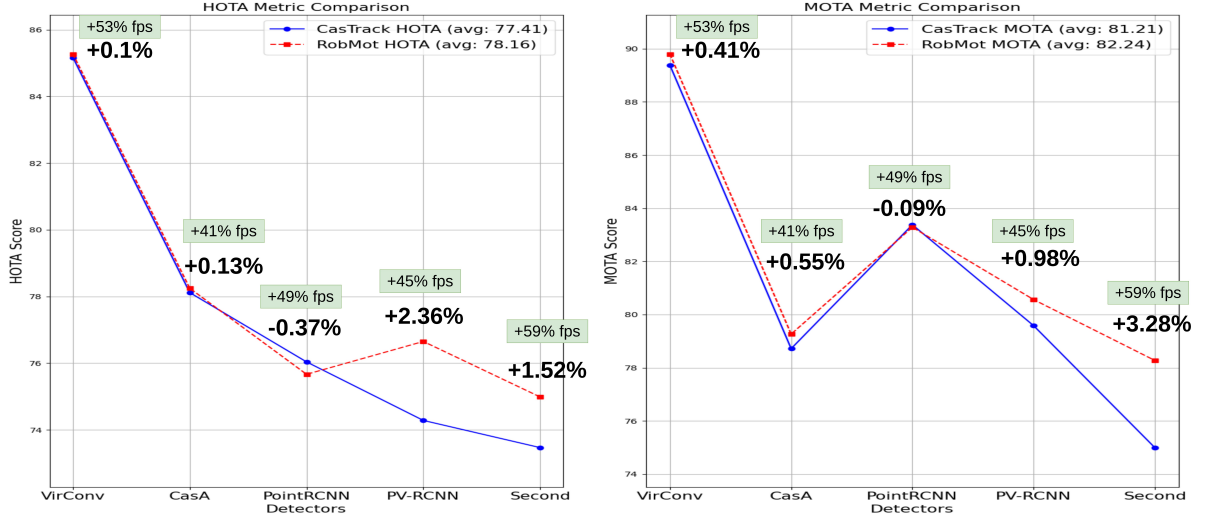


Figure 5: Tracking performance comparison on KITTI dataset *validation split* with CasTrack [1] across five different detectors: VirConv [18], CasA [19], PointRCNN [21], PV-RCNN [22], and Second [20]. We also report the gain in frame-per-second (fps). We observe that our framework exhibits a minimum **40% increase** in speed across all detectors.

drop in the CasTrack [1] performance by switching the detector. The drop reaches 2.4% in HOTA with PV-RCNN detector and 3.2% in MOTA with Second detector. Although changing detection performance could result in losing objects that eventually impact the tracking performance, our framework shows consistency across the detectors, as shown in Figure 5, in both HOTA and MOTA compared to CasTrack [1], when the performance drop does not exceed 1% with CasTrack [1], PointRCNN detector. The framework outperforms CasTrack [1] in four detectors in both HOTA and MOTA, with an average performance of 78.16% and 82.24% compared to CasTrack’s 77.41% and 81.21%, respectively. Notably, our framework’s frame-per-second processing is at least 40% higher than CasTrack [1] when both trackers are run on the same machine, which shows the framework’s efficiency.

#### 4.1.2 Qualitative Evaluation

One of the work’s significant contributions is mitigating the trajectory drift caused by noise associated with detections. The drift mitigation allows object retrievals after prolonged occlusions, frequent occlusions, or distortion in the observation. Figure 6 shows two challenging scenarios in MOT compared with CasTrack [1] as a top-performing tracker using the same detector. In the first scenario, in the first two rows, a distant car (ID:41) faces multiple occlusions and distortion in detection due to the distance. Our framework can maintain precise localization of the car along the subsequent occlusions and detection distortion, as shown in frame 187. The framework successfully tracks the car for about 90 consecutive frames, while CasTrack [1] loses the car at frame 61. In the second scenario, in the last two rows, a distant car (ID:3) is occluded by a building for about 50 frames. Despite the prolonged occlusion, our framework shows its substantial performance by successfully maintaining its trajectory during the occlusion and precisely estimating the car state, as shown in frames 102 and 107. The framework re-identifies the car at frame 110 and re-assigns its trajectory, while CasTrack [1] identifies it as a new car. These two scenarios affirm the substantial performance of the framework in prolonged occlusions.

#### 4.2 Ablation Study

This section demonstrates the effectiveness of our solutions for trajectory deviation and ghost tracks by studying concerns raised in this work and the proposed solution’s contribution to tackling them.



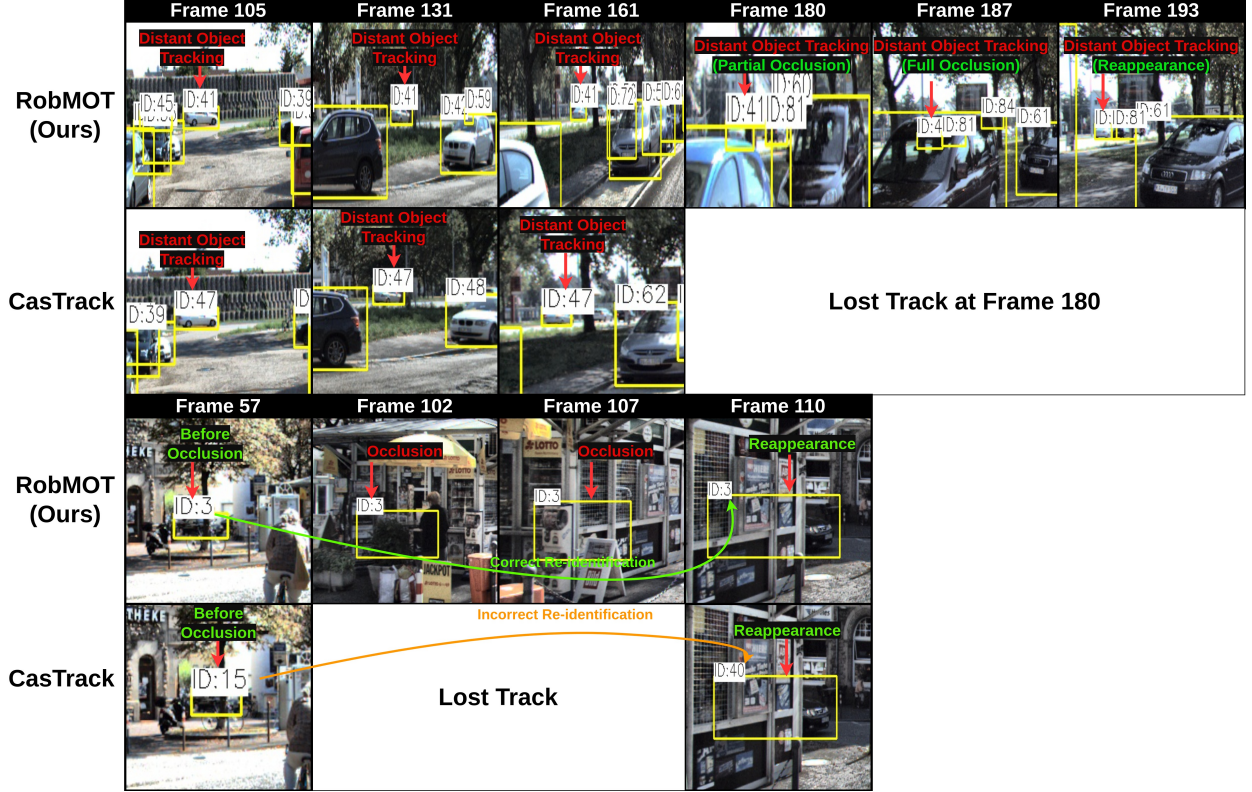


Figure 6: A qualitative evaluation of our framework performance with CasTrack [1] in two challenging multi-object tracking scenarios by projecting 3D tracking results into 2D frames. The first two rows show a scenario where a distant car (*ID:41*) faces multiple occlusions and distortion in detection. The second two rows show a scenario of a car (*ID:3*) occluded by a building for about 50 consecutive frames. Our framework tracks the distant car in the first scenario under distortion in the observation and occlusions while providing precise state estimation of the prolonged occluded car in the second scenario with successful recovery after the occlusion.

#### 4.2.1 Trajectory Drift

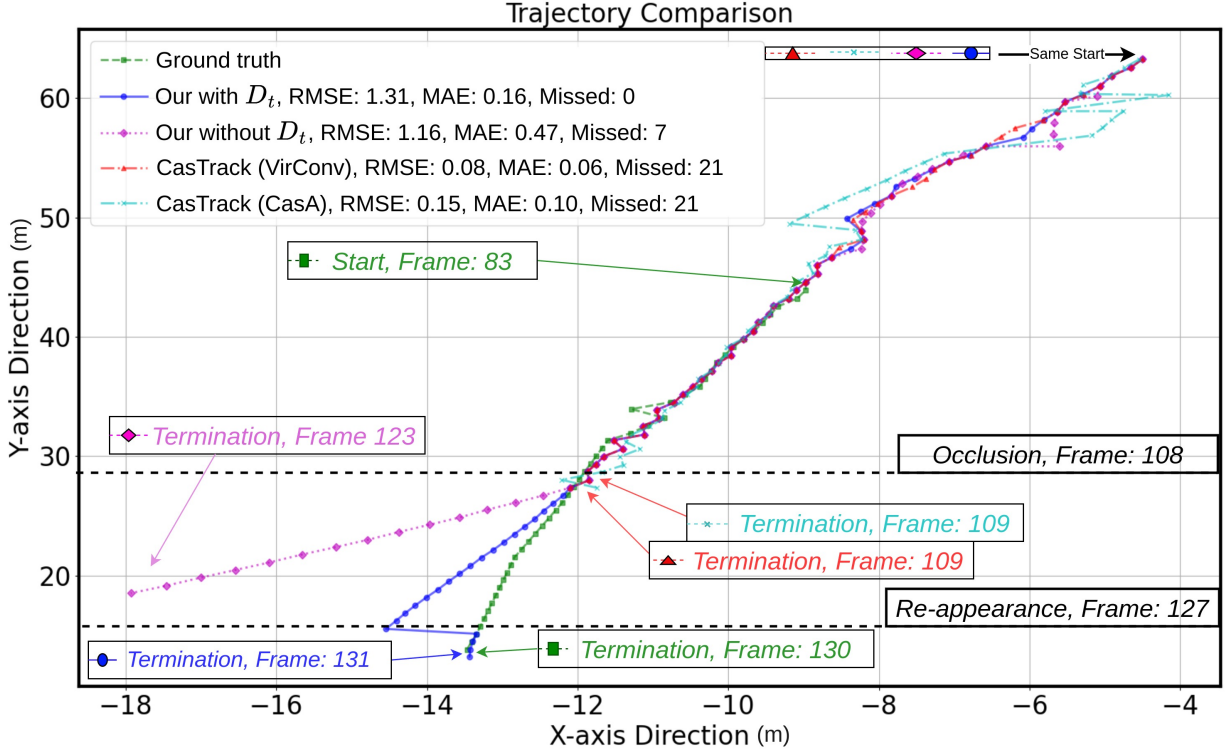


Figure 7: State estimation comparison of a trajectory for a car temporarily occluded in stream 0013 in the KITTI dataset. The **green** trajectory is the actual car’s trajectory. The **red** trajectory is CasTrack [1] with VirConv [18] detector. The **light blue** trajectory is CasTrack [1] with CasA [19] detector. The **pink** trajectory is our framework without trajectory drift mitigation noise. The **blue** trajectory is our framework with trajectory drift mitigation. While the pink trajectory suffered from the fluctuation noise and failed to recover the car, the proposed noise mitigation, the blue trajectory, reduced the drift in state estimation, allowing the car to be recovered after the occlusion.

This research raises concern about trajectory drift caused by spatial fluctuation noise associated with incoming detections. Figure 7 shows a car occluded and reappeared after about 20 frames. The graph contains five trajectories: one trajectory from the ground truth, two trajectories from CasTrack [1] with two different detectors, CasA [19] and VirConv [36], and two trajectories from our framework with and without the purposed drift mitigation solution. At the beginning, all car trajectories start simultaneously except the ground truth that initiates the trajectory at frame 83. When the car faces occlusion at frame 108, CasTrack [1] terminates the car trajectory in both detectors at frame 109. The trajectory of our framework without the proposed mitigation, pink color, suffers from high deviation from the actual car trajectory, resulting in trajectory termination. On the other hand, the trajectory with the mitigation term  $D_t$  has less deviation from the actual trajectory, allowing retrieving the car when it appears at frame 127. Despite the deviation in the mitigation solution, the graph shows that the car has changed its trajectory during the occlusion, which affirms that the deviation in the blue trajectory is relatively slim.

#### 4.2.2 Track Validity and Ghost Tracks

The second concern raised in this research is ghost tracks and the problem of relying on static detection thresholds followed in the literature, which cause leaks of ghost observations and block legitimate observations. To demonstrate the contribution of the observational gate and track validation stages in the work, we deactivate these two stages in the framework and compare five detectors with variant detection performance. To fairly apply the comparison, we deactivated the observational gate in Figure 2 by making  $\sigma_{conf}$  equals to  $\sigma_{nconf}$ . Thus, no further filtration will happen to the observations other than the standard detection threshold, as followed in the literature. The Trajectory Validity stage in Figure 2 is deactivated to prevent temporal identifications for ghost tracks. The top section of Table 3 shows the performance in HOTA and MOTA by these settings and the number of ghost tracks (IDFP) that appear. The bottom

Table 3: Performance evaluation of our framework with/without the proposed trajectory validity mechanism across five detectors

Method	Detector	HOTA $\uparrow$	MOTA $\uparrow$	IDFP $\downarrow$	HOTA Inc. $\uparrow$	FP Dec. $\downarrow$
RobMOT Without Track validity and obs. gate	PointRCNN [21]	68.67%	60.95%	2835	-	-
	PV-RCNN [22]	73.47%	72.53%	1164	-	-
	Second [20]	71.94%	69.67%	1179	-	-
	CasA [19]	76.86%	76.346%	743	-	-
	VirConv [18]	84.93%	89.43%	346	-	-
RobMOT With Track validity and obs. gate	PointRCNN [21]	75.67%	83.28%	552	+7%	-80%
	PV-RCNN [22]	76.65%	80.56%	658	+3.18%	-43%
	Second [20]	74.99%	78.27%	577	+3.05%	-51.1%
	CasA [19]	78.24%	79.26%	284	+1.38%	-61.8%
	VirConv [18]	85.26%	89.79%	227	+0.43%	-34.4%

section of Table 3 shows the framework with the proposed ghost tracks filtration mechanism. The solution shows improvement in HOTA and MOTA across all detectors, reaching 7% in HOTA, while decreasing 80% of the ghost tracks the traditional approach appeared. The study reveals that the impact of our proposed solution is emphasized with low-performing detectors, as shown in Table 3, which indicates the strength of the proposed mechanism and its contribution to the field.

## 5 Conclusion

This work discusses a noise associated with incoming detections that leads to drift in the state estimation of the objects. This noise comes from the spatial fluctuation of the detected bounding box and impacts the trajectories of occluded objects, preventing their recovery. Another type of noise is formed from false positive observations that lead to ghost tracks. While the literature relies on static thresholds to filter observations contributing to these tracks, it still leaks false observations and blocks observation of legitimate tracks, eventually impacting tracking performance. This research proposes a RobMOT framework that tackles the abovementioned challenges. Initially, adapting Kalman filter to drift noise mitigates trajectory drifting. Next, introduce a filtration mechanism for the ghost tracks by developing a temporal certainty about the track validity. Our solution outperforms the latest MOT benchmarks in KITTI and Waymo datasets, demonstrating its robustness across various detection performances, with a margin of about 3.2%. The framework qualitatively shows its substantial tracking performance for distant and recovering prolonged occluded objects while benchmarks fail. An ablation study has been conducted to demonstrate the contribution of the proposed solution in tracking performance. The study shows the mitigation in the drift impacting the state estimation of occluded objects as well as the capability of the framework to filter up to 80% of the leaked ghost tracks from the traditional filtration approach in the literature, enhancing the HOTA metric by 7%. The framework shows its applicability to real-time solutions with CPU constraints.

### 5.1 Future Work

Although our work shows mitigation in the trajectory deviation for occluded objects, allowing precise spatial state estimation of occluded objects and re-identifying them after the occlusion, this noise requires an intensive investigation as its implications on the state estimation observed on the benchmarks and how its reduction allows overcoming the challenging problem in tracking such as occlusion and distant objects. Even though this work considers the implication of this noise consistent on all objects, we will study the potential of modeling this noise dynamically to be developed up to the evolution of the object states in the environment.

## References

- [1] Wu et al. 3d multi-object tracking in point clouds based on prediction confidence-guided data association. *IEEE Transactions on Intelligent Transportation Systems*, 2022.
- [2] Xiyang Wang, Chunyun Fu, Zhankun Li, Ying Lai, and Jiawei He. Deepfusionmot: A 3d multi-object tracking framework based on camera-lidar fusion with deep association. *IEEE Robotics and Automation Letters*, 7(3):8260–8267, 2022.

- [3] Aleksandr Kim, Aljoša Ošep, and Laura Leal-Taixé. Eagermot: 3d multi-object tracking via sensor fusion. In *2021 IEEE International Conference on Robotics and Automation (ICRA)*, pages 11315–11321, 2021.
- [4] Liang Hu, Taihui Li, Nannan Xie, and Jiejun Hu. False positive elimination in intrusion detection based on clustering. In *2015 12th International Conference on Fuzzy Systems and Knowledge Discovery (FSKD)*, pages 519–523, 2015.
- [5] Leichen Wang, Jiadi Zhang, Pei Cai, and Xinrun Lil. Towards robust reference system for autonomous driving: Rethinking 3d mot. In *2023 IEEE International Conference on Robotics and Automation (ICRA)*, pages 8319–8325, 2023.
- [6] Jinkun Cao, Jiangmiao Pang, Xinshuo Weng, Rawal Khirodkar, and Kris Kitani. Observation-centric sort: Rethinking sort for robust multi-object tracking. In *Proceedings of the IEEE/CVF Conference on Computer Vision and Pattern Recognition (CVPR)*, pages 9686–9696, June 2023.
- [7] Kaer Huang, Kanokphan Lertniphonphan, Feng Chen, Jian Li, and Zhepeng Wang. Multi-object tracking by self-supervised learning appearance model. In *Proceedings of the IEEE/CVF Conference on Computer Vision and Pattern Recognition*, pages 3162–3168, 2023.
- [8] Jiarui Cai, Mingze Xu, Wei Li, Yuanjun Xiong, Wei Xia, Zhuowen Tu, and Stefano Soatto. Memot: Multi-object tracking with memory. In *Proceedings of the IEEE/CVF Conference on Computer Vision and Pattern Recognition*, pages 8090–8100, 2022.
- [9] Pavel Tokmakov, Jie Li, Wolfram Burgard, and Adrien Gaidon. Learning to track with object permanence. In *Proceedings of the IEEE/CVF International Conference on Computer Vision*, pages 10860–10869, 2021.
- [10] Tim Meinhardt, Alexander Kirillov, Laura Leal-Taixe, and Christoph Feichtenhofer. Trackformer: Multi-object tracking with transformers. In *Proceedings of the IEEE/CVF conference on computer vision and pattern recognition*, pages 8844–8854, 2022.
- [11] Chaoda Zheng, Xu Yan, Haiming Zhang, Baoyuan Wang, Shenghui Cheng, Shuguang Cui, and Zhen Li. Beyond 3d siamese tracking: A motion-centric paradigm for 3d single object tracking in point clouds. In *Proceedings of the IEEE/CVF Conference on Computer Vision and Pattern Recognition*, pages 8111–8120, 2022.
- [12] Jeongseok Hyun, Myunggu Kang, Dongyoon Wee, and Dit-Yan Yeung. Detection recovery in online multi-object tracking with sparse graph tracker. In *Proceedings of the IEEE/CVF Winter Conference on Applications of Computer Vision*, pages 4850–4859, 2023.
- [13] Gianluca Mancusi, Aniello Panariello, Angelo Porrello, Matteo Fabbri, Simone Calderara, and Rita Cucchiara. Trackflow: Multi-object tracking with normalizing flows. In *Proceedings of the IEEE/CVF International Conference on Computer Vision*, pages 9531–9543, 2023.
- [14] Yuang Zhang, Tiancai Wang, and Xiangyu Zhang. Motrv2: Bootstrapping end-to-end multi-object tracking by pretrained object detectors. In *Proceedings of the IEEE/CVF Conference on Computer Vision and Pattern Recognition*, pages 22056–22065, 2023.
- [15] Kaer Huang, Kanokphan Lertniphonphan, Feng Chen, Jian Li, and Zhepeng Wang. Multi-object tracking by self-supervised learning appearance model. In *2023 IEEE/CVF Conference on Computer Vision and Pattern Recognition Workshops (CVPRW)*, pages 3163–3169, 2023.
- [16] Gianluca Mancusi, Aniello Panariello, Angelo Porrello, Matteo Fabbri, Simone Calderara, and Rita Cucchiara. Trackflow: Multi-object tracking with normalizing flows. In *Proceedings of the IEEE/CVF International Conference on Computer Vision (ICCV)*, pages 9531–9543, October 2023.
- [17] Mohamed Nagy, Majid Khonji, Jorge Dias, and Sajid Javed. Dfr-fastmot: Detection failure resistant tracker for fast multi-object tracking based on sensor fusion. In *2023 IEEE International Conference on Robotics and Automation (ICRA)*, pages 827–833, 2023.
- [18] Wu et al. Virtual sparse convolution for multimodal 3d object detection. In *Proceedings of the IEEE/CVF Conference on Computer Vision and Pattern Recognition (CVPR)*, June 2023.
- [19] Wu et al. Casa: A cascade attention network for 3-d object detection from lidar point clouds. *IEEE Transactions on Geoscience and Remote Sensing*, 2022.
- [20] Yan Yan, Yuxing Mao, and Bo Li. Second: Sparsely embedded convolutional detection. *Sensors*, 18(10):3337, 2018.
- [21] Shaoshuai Shi, Xiaogang Wang, and Hongsheng Li. Pointcnn: 3d object proposal generation and detection from point cloud. In *The IEEE Conference on Computer Vision and Pattern Recognition (CVPR)*, June 2019.

- [22] Shaoshuai Shi, Chaoxu Guo, Li Jiang, Zhe Wang, Jianping Shi, Xiaogang Wang, and Hongsheng Li. Pv-rcnn: Point-voxel feature set abstraction for 3d object detection. In *Proceedings of the IEEE/CVF Conference on Computer Vision and Pattern Recognition (CVPR)*, June 2020.
- [23] Andreas Geiger, Philip Lenz, and Raquel Urtasun. Are we ready for autonomous driving? the kitti vision benchmark suite. In *Conference on Computer Vision and Pattern Recognition (CVPR)*, 2012.
- [24] Jonathon Luiten, Aljosa Osep, Patrick Dendorfer, Philip Torr, Andreas Geiger, Laura Leal-Taixe, and Bastian Leibe. Hota: A higher order metric for evaluating multi-object tracking. *International Journal of Computer Vision (IJCV)*, 2020.
- [25] Pei Sun, Henrik Kretschmar, Xerxes Dotiwalla, Aurélien Chouard, Vijaysai Patnaik, Paul Tsui, James Guo, Yin Zhou, Yuning Chai, Benjamin Caine, Vijay Vasudevan, Wei Han, Jiquan Ngiam, Hang Zhao, Aleksei Timofeev, Scott Ettinger, Maxim Krivokon, Amy Gao, Aditya Joshi, Yu Zhang, Jonathon Shlens, Zhifeng Chen, and Dragomir Anguelov. Scalability in perception for autonomous driving: Waymo open dataset. In *2020 IEEE/CVF Conference on Computer Vision and Pattern Recognition (CVPR)*, pages 2443–2451, 2020.
- [26] Hai Wu, Qing Li, Chenglu Wen, Xin Li, Xiaoliang Fan, and Cheng Wang. Tracklet proposal network for multi-object tracking on point clouds. In Zhi-Hua Zhou, editor, *Proceedings of the Thirtieth International Joint Conference on Artificial Intelligence, IJCAI-21*, pages 1165–1171. International Joint Conferences on Artificial Intelligence Organization, 8 2021. Main Track.
- [27] Ziming Zhu, Jiahao Nie, Han Wu, Zhiwei He, and Mingyu Gao. Msa-mot: Multi-stage association for 3d multimodality multi-object tracking. *Sensors*, 22(22):8650, 2022.
- [28] Hai Wu, Wenkai Han, Chenglu Wen, Xin Li, and Cheng Wang. 3d multi-object tracking in point clouds based on prediction confidence-guided data association. *IEEE Transactions on Intelligent Transportation Systems*, 23(6):5668–5677, 2022.
- [29] Andreas Reich and Hans-Joachim Wuensche. Monocular 3d multi-object tracking with an ekf approach for long-term stable tracks. In *2021 IEEE 24th International Conference on Information Fusion (FUSION)*, pages 1–7, 2021.
- [30] Aleksandr Kim, Guillem Brasó, Aljoša Ošep, and Laura Leal-Taixé. Polarmot: How far can geometric relations take us in 3d multi-object tracking? In Shai Avidan, Gabriel Brostow, Moustapha Cissé, Giovanni Maria Farinella, and Tal Hassner, editors, *Computer Vision – ECCV 2022*, pages 41–58, Cham, 2022. Springer Nature Switzerland.
- [31] Nicola Marinello, Marc Proesmans, and Luc Van Gool. Triplettrack: 3d object tracking using triplet embeddings and lstm. In *Proceedings of the IEEE/CVF Conference on Computer Vision and Pattern Recognition*, pages 4500–4510, 2022.
- [32] Qitai Wang, Yuntao Chen, Ziqi Pang, Naiyan Wang, and Zhaoxiang Zhang. Immortal tracker: Tracklet never dies. *arXiv preprint arXiv:2111.13672*, 2021.
- [33] Ziqi Pang, Zhichao Li, and Naiyan Wang. Simpletrack: Understanding and rethinking 3d multi-object tracking. In *ECCV Workshops*, 2021.
- [34] Tianwei Yin, Xingyi Zhou, and Philipp Krahenbuhl. Center-based 3d object detection and tracking. In *Proceedings of the IEEE/CVF Conference on Computer Vision and Pattern Recognition (CVPR)*, pages 11784–11793, June 2021.
- [35] Yihan Zeng, Chao Ma, Ming Zhu, Zhiming Fan, and Xiaokang Yang. Cross-modal 3d object detection and tracking for auto-driving. In *2021 IEEE/RSJ International Conference on Intelligent Robots and Systems (IROS)*, pages 3850–3857, 2021.
- [36] *Scenario Trajectory Deviation Cause of Det. Noise 00:01:38, Supplied as supplemental material Demo.mp4.*